# Detecting John Cunningham Virus Translocations through Solid-State Nanopores

Oliver G. Isik
Advisor: Prof. Derek Stein

# Contents

# List of Figures

CHAPTER 1

# Introduction

Biophysics is concerned with the underlying physical mechanisms of biological phenomena; one active area of current research is the detection of individual biomolecules and determination of those polymers' physical properties and individual behaviors. To create an apparatus to detect them, knowledge of nanotechnology is not only useful, but also required. The average eukaryotic cell is 25 $\mu$m in diameter—though the variation depending on cell type is not insigificant—with organelles an order of magnitude smaller, and individual biomolecules one or more orders of magnitude smaller than that. Many techniques used to detect these macromolecules are based off the methods that biological systems themselves use to detect and identify the presence of specific substrates.

Biological systems maintain their environments through the use of phospholipid membranes, controlling the translocation of macromolecules across these membranes through the use of pores only nanometers in diameter. Often times, these pores are stabilized by the presence of transmembrane proteins, and sometimes they are created by gap junctions that allow for diffusion of ions between neighboring epithelial cells. Cells are also capable of detecting when specific ligands translocate through a specific membrane pore—usually with the help of enzymes bound to the inside of the pore—and signal a specific intracellular response upon sensing such an event. The intracellular response is called a signal transduction pathway, and can have a variety of effects that range from promoting increased glucose uptake for metabolism to initiating apoptosis, or controlled degradation of cellular contents. Thorough understanding of these pathways is essential to both our scientific knowledge of cell biology and the development of pharmacological treatments in medicine.

Developing an apparatus as sophisticated and precise as those membrane cell receptors found in biological systems has become a great interest for scientists. Recently, scientists have developed techniques of detecting specifically when macromolecules translocate through an isolated biological membrane by measuring changes in electrical current across the open pores. Relative to the salt solution in which they are immersed, the biomolecules are more electrically resistive, and the measured electrical current decreases during translocations. The shape of these signals on a graph of current against time is determined by the electric fields and pressure gradients applied, the relative conductivities of the solution and biomolecules, and the shape of the membrane pore. Analysis of these signals provides insight into the physical properties of the biomolecules, including charge density, length, and size. Additionally, by translocating biomolecules whose properties are well-understood, one can determine physical properties of a nanopore.

The Stein lab uses solid-state materials for nanopores, most commonly silicon nitride membranes, chemically fabricated to have pore diameters as small as 1–10 nm and lengths of less than 100 nm. Solid-state nanopores have previously been successful in detecting the translocation of double-stranded deoxyribonucleic acid (DNA) molecules [7]. More recently, the Stein lab has used them to detect the filamentous *fd* virus [12] and the capture patterns of $\lambda$-DNA [13].

DNA and filamentous viruses, the two main biomolecules the Stein lab has been successful at detecting using solid-state nanopores, are both linear in shape, and much longer than the nanopore. Thus, the duration that any one part of the molecule occludes the pore is greater, making the translocation event easier to detect. This longer translocation time can be seen in longer periods of decreased electrical current, which better distinguishes signals from noise.

However, not all biomolecules are filamentous, and small, globular molecules abound in biological systems. Biomolecules can speed through nanopores at rates too fast for polymers this small to be detectable using current nanotechnology. Recent tests of solid-state nanopores detecting translocations of small, globular proteins have shown that successful detections require slowing down the particles enough to make the translocation durations measurable. In these experiments, the groups found they were only detecting the translocations of the slowest proteins [17], the quicker ones passing through the pore too quickly to show on a graph.

This project has aimed to refine the nanopore as a sensor for the 45-nm diameter, spherical John Cunningham Virus. The John Cunningham virus is a human polyomavirus linked to progressive multifocal leukoencephalopathy, a disorder causing demyelination of neural axons in the human central nervous system [11]. For our source of virus particles, we used an aliquot of John Cunningham Pseudovirus constructs donated to the Stein lab by the Walter Atwood Molecular Virology Lab.

Using a conventional nanopore of length 50 nm and the standard applied voltage of 100 mV in nanopore experiments, each translocation would be shorter than 1 $\mu$s, too short in duration to be detected by our nanoelectronics system; the system's analog current-to-voltage amplifier has a 50 kHz filter that filters out any signal less than 20 $\mu$s. Thus, the main task of the project has been to devise an apparatus and experimental procedure that increases translocation durations by several orders of magnitude. By designing a new fluidic cell to better control the applied voltages and pressure gradients that influence velocity of virus translocation, manipulating the geometry of the nanopores, and optimizing the chemical properties of the fluid in which the viruses are immersed, we have developed methods to slow the motion of the virus particles and make the translocations of the John Cunningham Virus detectable using solid-state nanopores.

CHAPTER 2

# Theoretical Models of Virus Translocations through Extended Solid-State Nanopores

In order to detect the translocation of virus particles through a nanopore sensor, the electrical current signal has to be distinguishable from noise. Two key ways to make the signal more visible are to increase its duration and to increase its strength. One additional consideration that becomes necessary when the virus particles are smaller than the pores used is the frequency of translocation; in order to ensure accurate results, we have to ensure that the signals being created are from a single virus particle's translocation, not multiple simultaneous translocations that cause an apparent increase in signal strength and duration.

Therefore, the variables of interest in modeling the translocation of a spherical virus through a nanopore are the velocity of the particle as it passes through the pore—and its conjugate variable, the time the virus actually spends in the pore—how frequently viruses can be expected to translocate, and how much a virus can be expected to alter the current passing through the pore during translocation. Knowing these three parameters gives an estimate of the duration, frequency, and strength of signals the translocation will present, which provides insight into whether we can detect such a translocation using our nanopore apparatus. Furthermore, knowing how different chemical and physical properties of the system affect these parameters of interest allows us to manipulate them in a manner that best promotes detection of virus translocations. The chemical and physical properties of our apparatus are provided in Table 1.

| Variable | Description | Value in Conventional Nanopore Experiments | Value in Our Modified Nanopore Apparatus |
|---|---|---|---|
| $\epsilon$ | dielectric constant | 80 | 80 |
| $\zeta_{\text{pore}}$ | pore $\zeta$-potential | varies | $-50\,\text{mV}$ |
| $\zeta_{\text{virus}}$ | virus $\zeta$-potential | — | $10\,\text{mV}$ |
| $\eta$ | viscosity | $10^{-3}\,\text{Pa}\cdot\text{s}$ | $10^{-3}\,\text{Pa}\cdot\text{s}$ |
| $a$ | virus radius | — | $22.5\,\text{nm}$ |
| $r_0$ | pore radius | 1–100 nm | $30\,\text{nm}$ |
| $\ell$ | pore length | 1–10 nm | $100\,\text{nm}$ |
| $\Delta V$ | applied voltage | 10–1000 mV | $50\,\text{mV}$ |
| $\Delta P$ | applied pressure | varies | $5\,\text{kPa}$ |
| $\sigma$ | sol'n conductivity | varies | $50\,\text{mS/cm}$ |

Table 1. The variables representing chemical and physical properties of the apparatus that are used in this chapter. The values used in our calculations below, which are roughly equivalent to those used in our experiments, are compared to those used in conventional nanopore experiments.

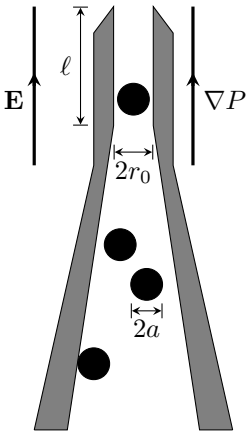


FIGURE 2.1. Diagram of nanopore capillary with John Cunningham Virus particles submerged; the depicted electric field direction is reversible, but the pressure gradient direction is not in our apparatus without forcing air into the nanopore.

## 1. Forces Governing Virus Translocation

We model virus translocations in terms of the effects of four forces on the motion of the particle. Two forces, electrophoresis and electro-osmosis, are created by the application of an external electric field across the nanopore. Another force is created by application of a pressure gradient across the fluidic cell, which causes a Poiseuille flow within the nanopore. Finally, Brownian motion of virus particles is accounted for in determining the translocation velocity.

**1.1. Electrokinetic Effects.** The application of an external electric field creates two forces that act in opposite directions: electrophoresis and electro-osmosis [4]. In electrophoresis, the balance between the electrostatic force on the charged virus and the viscous drag force of the fluid causes motion of the virus particle relative to the fluid. In electro-osmosis, an electric field induces bulk flow of the electrically-charged fluid near the surface of the nanopore, and that flow carries virus particles with it. Combining the two effects gives a formula for virus translocation velocity. The velocity of the virus is proportional to the magnitude of the applied electric field, and is called the slip speed or the Smoluchowski speed [4].

$$v_{\text{slip}} = \frac{\epsilon\epsilon_0\zeta_{\text{virus}}}{\eta\ell}\Delta V \tag{2.1}$$

where $\epsilon_0 = 8.85 \times 10^{-12}\,\text{F/m}$ is the vacuum permittivity. The quantity $\zeta_{\text{pore}}$ is called the electrokinetic potential, or $\zeta$-potential, of the virus particle and is an indirect measure of the effective charge density [4]. The equation for electro-osmosis is similar, but its flow lines exponentially decay near the surface of the nanopore, as shown in Fig. 2.2a [4].

$$v_{\text{osmosis}} = -\frac{\epsilon\epsilon_0\zeta_{\text{pore}}}{\eta\ell}(1 - e^{-\kappa z})\Delta V \tag{2.2}$$

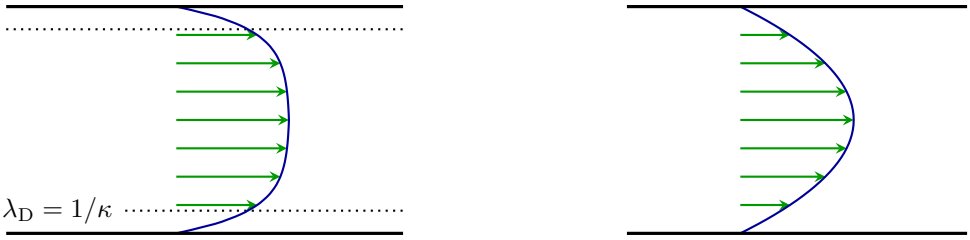


(A) Electrokinetic flow lines. (B) Poiseuille flow lines.

FIGURE 2.2. Flow lines of the electrokinetic effects and the Poiseuille flow within the nanopore, expressed as a function of the distance to the edge of the nanopore. Electrokinetic flow lines decay exponentially as the distance to the edge of the pore decreases, with a decay constant of the Debye length; Poiseuille flow lines decay quadratically.

$z$ is the distance of the virus from the perimeter of the pore, and $\kappa = 1/\lambda_D$ is the inverse of the Debye length, the length scale over which the electro-osmotic effects are observed. $\zeta_{virus}$ is the electrokinetic potential of the nanopore surface [4].

Calculating the composite effects of the Smoluchowski speed and electro-osmotic flow at the center of the nanopore—ignoring the nonlinear effects and thus the exponential term in Eq. (2.2)—gives an estimate of the electrokinetic effects on velocity. Given that the Debye length is of order of magnitude 1 nm, we can assume $e^{-\kappa r_0} \ll 1$ and the nonlinear effects can be ignored. For the parameters of our experiment, which are detailed in Table 1, the velocity is approximately 4 mm/s. Such a velocity would give a translocation duration of 30 $\mu$s, which is slow enough to pass through the 50-kHz filter and show on a readout of current versus time. For a conventional nanopore of length 1–10 nm, that time would be closer to 100–500 ns and would be undetectable, illustrating the need for longer nanopores in our experiments.

**1.2. Poiseuille Flow.** When analyzing the fluid dynamics of the system, we can assume that all fluid flows are laminar at the microscopic scale. This claim is supported by the Reynolds number, a dimensionless quantity whose value is small for laminar flows and large for turbulent flows. The Reynolds number of the 45-nm diameter John Cunningham Virus moving at a velocity of 1 mm/s through water can be calculated as $R = \rho_w v a/\eta = 5 \times 10^{-5}$ [18]. Such a small value says that fluid flow is laminar, and no turbulent effects need to be considered [18].

Under a pressure gradient, the viscous fluid flows from high to low pressure, carrying virus particles with it [10]. Under a pressure difference $P$, the velocity of the fluid through a cylindrical tube of radius $r_0$ and length $\ell$ is given by the Hagen-Poiseuille equation and is a function of the distance $z$ from the surface of the inside of the nanopore ($0 \leqslant z \leqslant r_0$) [10]:

$$v = \frac{z^2}{4\eta\ell}\Delta P \tag{2.3}$$

With the parameters in Table 1, the velocity of the Poiseuille flow is roughly 6 mm/s, producing a translocation time of 20 $\mu$s; This duration is the shortest signal detectable by our nanoelectronics equipment. Conventional nanopores with lengths on the order of 1-10 nm would give signal durations several orders of magnitude shorter, which would be undetectable using our nanoelectronics software, once again demonstrating the need for elongated capillary nanopores. Furthermore, even with our extended nanopores, in combination with an applied electric field, the pressure difference and the voltage must both be decreased in magnitude or applied in opposite directions; otherwise, the virus will translocate in fewer than 20 $\mu$s, and the signal will be undetectable. If the 5-kPa pressure is applied in the opposite direction as the 50-mV potential difference, the particle velocity would be 2 mm/s, doubling the translocation time

**1.3. Simple Diffusion.** Spherical virus particles exhibit Brownian motion, diffusing throughout an aqueous solution in which they are submerged. Simple diffusion, when considered in one dimension, can be modeled from the equation of Brownian motion, a solution to the diffusion equation [20]:

$$\langle \Delta x^2 \rangle = 2Dt \tag{2.4}$$

where $D$, the diffusion constant, can be further calculated for a virus particle of radius $a$ by the Einstein-Stokes relation for the diffusion constant of a spherical particle exhibiting laminar flow through a fluid [21]:

$$D = \frac{k_{\mathrm{B}}T}{6\pi a\eta} \tag{2.5}$$

where $T$ is the temperature and $k_{\mathrm{B}} = 1.38\times10^{-23}$ J/K is Boltzmann's constant. Approximating $\langle \Delta x^2 \rangle^{1/2} = \ell$ provides a translocation velocity $v = \ell/t$ of

$$v = \frac{k_{\mathrm{B}}T}{3\pi\eta a\ell} \tag{2.6}$$

At room temperature (approximately 300 K), the velocity from simple diffusion is roughly 200 $\mu$m/s, which gives a translocation duration of 500 $\mu$s. For the lengths of pores we are using in this experiment, the contribution of Brownian Motion to virus particle velocity is roughly an order of magnitude smaller than that induced by electrokinetic effects or Poiseuille flow, and therefore simple diffusion plays a much smaller role than the other factors in determining translocation velocity.

It should be noted that this model of simple diffusion is necessarily incomplete for a few reasons. This model is one-dimensional, and in reality a nanopore is naturally three-dimensional. Additionally, the nanopores used in this system are not cylindrical; they are conical, and that means that diffusion is not equally favored in either direction. A modified model of diffusion, one that takes entropic effects into more consideration, is required for a more accurate estimate of the effects of diffusion on particle velocity in the

direction of translocation. Such models can be achieved through approximate solutions to the Fick-Jacobs equation, a modified diffusion equation that accounts for variations in cross-sectional area over the length of a pore [19]. However, given how small the conical angle is on the capillaries used, it is unlikely that such entropic effects will change estimates by an order of magnitude, and therefore we did not calculate them.

**1.4. Translocation Frequency.** The frequency of translocations in nanopore experiments is often approximated by the Smoluchowski Rate Equation [17], which is based on a solution of the diffusion equation. Particles' trajectories are heavily influenced by Brownian motion before they reach the pore, but once a particle enters the opening of the pore, the other forces created by electrokinetic effects and Poiseuille flow take over.

According to the Smoluchowski Rate Equation, the frequency of virus translocations $J$ is proportional to the concentration of viruses $\rho$ and the diffusion constant $D$ [17]:

$$J = 2\pi r_0 D\rho = \frac{k_{\mathrm{B}} T r_0 \rho}{3a\eta} \tag{2.7}$$

For our experiments, this frequency is approximately $6\times10^{-4}$ translocations per second, which corresponds to about 1700 s—or 28 min—between consecutive translocations. However, the Smoluchowski Rate Equation is less of an estimate and more of a lower bound on the frequency of virus translocations for our experiments. As is shown in Fig. 2.1, the tapers on our nanopores are gradual, meaning that the electric field is nonnegligible proximal to the tip; this field can guide particles to the nanopore. As it was already shown that the electrokinetic effects contribute more to particle velocity than Brownian motion, these effects can be expected to greatly increase the frequency of particle translocation. The exact effect that the electrokinetic effects will have is dependent on the geometry of the nanopore's taper.

Understanding the rough dependence of translocation time and translocation frequency on each of these parameters allows us to refine the detector and control the variables that determine whether we can detect translocations. If each virus moves through too quickly, the extremely short signal will be filtered out by the apparatus's 50-kHz filter, and the signals would not be visible in the current output. If the viruses move through too frequently to the point that more than one is in the pore at a time, approximating signal strength is more difficult because one has to account for the difference in signal strength resulting from different numbers of virus particles in the process of translocation.

## 2. Effects of Virus Translocation on Electrical Current

The other variable of key interest is the strength of the electrical signal that can be expected from a virus translocation. The two variables that measure this strength are the absolute change in current, $\Delta I$, and the relative change against baseline current, $\Delta I/I_0$. Both the absolute magnitude of the change in

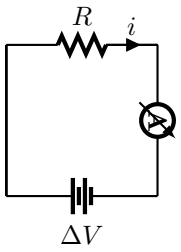


FIGURE 2.3. Model of nanopore as a resistor in a simple direct-current electrical circuit with or without a spherical particle translocating. In the high-conductivity limit, $\Delta R > 0,\ \Delta I < 0$; in the low-conductivity limit, $\Delta R < 0,\ \Delta I > 0$.

current and the comparison to baseline are important, since the latter gives a measure of relative change, but the former gives a measure of absolute change. If absolute change is not great enough, the signal will be indistinguishable from noise, which is not very dependent on the baseline current and in our experiments is usually of order $\delta I = \pm 30\,\mathrm{pA}$.

Both outputs can be calculated by modeling our system as a circuit and virus translocations as a change in the resistance of the nanopore, as shown in Fig. 2.3. According to Ohm's law, the current should change accordingly:

$$\Delta I = \frac{\Delta V}{R_0 + \Delta R} - \frac{\Delta V}{R_0} \tag{2.8}$$

and, when compared to the baseline current of $I_0 = \Delta V / R_0$:

$$\frac{\Delta I}{I_0} = \frac{\Delta R}{R_0 + \Delta R} \tag{2.9}$$

The baseline resistance can be modeled for a roughly cylindrical nanopore of radius $r_0$, length $\ell$, and filled with solution of conductivity $\sigma$:

$$R_0 = \frac{\ell}{\pi r_0^2 \sigma} \tag{2.10}$$

To model the change in resistance during virus translocations, we explore two limits: one in which the viruses are submerged in de-ionized water and are relatively conductive; and one in which the viruses are submerged in aqueous salt solutions and are relatively resistive. When the virus conductivity is much greater than that of the solution, the current will increase during translocations due to an increased net conductivity of the capillary. When the virus conductivity is much lower than that of the solution, the current will decrease during translocations due to a decreased net conductivity of the capillary.

**2.1. Resistive Pulse Technique for Saline Solutions.** In saline solutions, the current will decrease under the presence of the relatively resistive virus particle, given that the conductivity of 500 mM KCl is

50 mS/cm [6]. The common model used for determining the change in resistance upon the translocation of a spherical particle in the high solution conductivity limit is the Resistive Pulse Technique [6]:

$$\Delta R = \frac{2a^3}{\pi\sigma r_0^4}\left[1 + 6\left(\frac{r_0}{\ell}\right)^4 + \cdots\right] \tag{2.11}$$

which means that the change in current compared to baseline is given by:

$$\frac{\Delta I}{I_0} = 1 - \left\{1 + \frac{2a^3}{\ell r_0^2}\left[1 + 6\left(\frac{r_0}{\ell}\right)^4 + \cdots\right]\right\}^{-1} \tag{2.12}$$

According to the mathematical results of the Resistive Pulse Technique, as the length of the pore increases, the signal strength decreases. As the size of the virus particle increases, the signal strength approaches that of the baseline current.

Given the shape of our nanopores described above, using 500 mM KCl solution, we can approximate the change in current as approximately 1.5 nA, with a change against baseline of approximately 20%. Such a change should be detectable against a baseline current, and should also be much larger than any noise.

It should be noted that the resistive pulse technique was designed as a model for systems where $a \ll r_0$, a condition which is not necessarily applicable in these experiments. Therefore, this model offers less of a precise prediction and more of an order-of-magnitude estimate for the signal strength. However, given the number of confounding variables that can alter the experimental environment in minor ways, as well as the noise that is inherent in all electrical current measurements, an estimate of the order of magnitude is good enough to provide a rough idea of anticipated results.

A caveat to using highly conductive solution is that in the exceedingly high limit of salinity (1 M or 2 M), while the conductivity of the solution may increase and the signal strength will increase relative to the noise, the electrokinetic ($\zeta$) potential of the virus particles can decrease significantly [2]. Therefore, solutions between 200–500 mM are a safer intermediate.

**2.2. Low-Conductivity Solution.** In the lower limit of solution conductivity, we expect the current to increase under the presence of a relatively conductive virus, given that the conductivity of water is $\sigma = 55$ nS/cm and that virus particles are likely to contain enough surface charge density to drastically exceed that conductivity [2]. Upon addition of the virus particle (of radius $a$), the resistance can be approximated by decreasing the effective length of the resistor by the diameter of the virus particle:

$$\Delta R = -\frac{2a}{\pi r_0^2 \sigma} \tag{2.13}$$

Using Ohm's Law, we can approximate the change in current as

$$\Delta I = \pi r_0^2 \sigma V_0 \left(\frac{1}{\ell - 2a} - \frac{1}{\ell}\right) \tag{2.14}$$

To compare against baseline current:

$$\frac{\Delta I}{I_0} = \frac{1}{\ell/2a - 1} \tag{2.15}$$

This result is also a function only of the geometry of the virus and the length of the pore, showing that as the size of the virus increases, so does the change in current, and as the length of the pore increases, the signal strength decreases. Based on this result, in the low limit of solution conductivity, increasing the length of the pore can increase the translocation duration, which is helpful to being able to detect such a particle, but decreases the strength of the signal, which naturally makes it more difficult to detect translocations.

For our capillaries in this fluid environment, the change in current expected during John Cunningham Virus translocations is 6 fA, and the relative change over the baseline is roughly 82%. However, since this theoretical change is unreasonably difficult to detect against a noise $\delta I$ four orders of magnitude greater, very few experiments were actually run in deionized water; all successful trials were run in salt solutions.

**2.3. Effects of Pressure on Baseline Current.** Another consideration that must be taken into account is the effect of streaming current, or the effect in which a pressure gradient across a nanopore creates an electrical current [4]. This factor needs to be considered because it will change the baseline current, and translocation of a virus is likely to have little or no effect on the amplitude of the streaming current [9]; the relative strength of the signal compared to the baseline current is therefore dependent on the presence of this factor.

The streaming current is measured as [4, 9]:

$$i = \frac{\pi \epsilon \epsilon_0 r_0^2 \zeta}{\eta \ell} \Delta P \tag{2.16}$$

For the parameters of our experiment, the streaming current is approximately 1 pA, and can therefore be neglected as it is several orders of magnitude smaller than the baseline current created by an electric field applied across a 500 mM KCl solution.

Since the efficacy of nanopore sensors is dependent upon the ability to create an electrical current that responds to virus translocations in an appropriate manner, understanding the nuanced effects of the parameters of our experiment (applied voltage, applied pressure, pore diameter and length, virus diameter and $\zeta$-potential) on current allows us to further refine the sensor and optimize key properties. Our models allow us to roughly optimize nanopore length at approximately 100 nm, so that the duration is increased long enough to not be filtered out by the amplifier, but the signal intensity is not decreased so much that it is indistinguishable from noise.

CHAPTER 3

# Design of Experimental Apparatus

A typical nanopore measures 1–100 nm in diameter and 1–10 nm in length, commonly made from transmembrane protein channels in a lipid bilayer or pores carefully drilled into solid-state silicon nitride films using electrons or ions [7]. In nanopore experiments, particles to be translocated are injected into the apparatus on one side of the pore, and an electrode on each end connects each chamber to opposite ends of a power source, as shown in Fig. 3.1.

Due to the John Cunningham Virus's small size, Eq. 2.1 predicts that most will have translocation durations of less than 1 $\mu$s. These signals will be filtered out by the 50 kHz filter in our our electronics equipment's analog current-to-voltage amplifier, and the signal will not be detected. To solve this dilemma, we increase the length of our pores so that the particles spend 10–100 $\mu$s translocating. By increasing pore length, however, we decrease signal strength as well as baseline current, as indicated by the results given in Eq. (2.12), so creating a pore of diameter barely large enough to fit the 45-nm diameter John Cunningham Virus is important for optimizing the sensor; Eq. (2.11) predicts that in a relatively conductive solution, the larger the virus relative to the pore, the greater the increase in resistance and translocation signal strength. Minimizing diameter allows us to get away with longer pore lengths, achieving longer translocation durations without sacrificing too much signal strength.

In our experimental setup, we use a specialized fluidic cell designed specifically for this experiment. It is designed to stably hold a 5-cm glass capillary of outer diameter 1 mm, which tapers to a nanopore tip at one end. In addition to allowing us to apply an electric field across our nanopore, this fluidic cell allows us to control the pressure gradient, a key parameter of interest when we created our model of spherical virus translocations. We also use a modified style of nanopore, which is already used by the Stein lab for detecting translocations of carbon nanotubes and for the group's nanopore mass spectrometer project; these capillaries can be fabricated to longer, more optimal lengths and diameters for detecting the John Cunningham Virus.

## 1. Capillary Fabrication

To fabricate an extended nanopore tip from a glass capillary, the capillary must be heated in the middle and pulled at its ends to form two nanopore tips, as shown by the schematic in Fig. 3.2. By controlling the duration and intensity of heating, as well as the force and velocity with which the capillaries are pulled apart, we can change the pore's diameter and taper length. The final nanopores are 3.5–5-cm capillaries

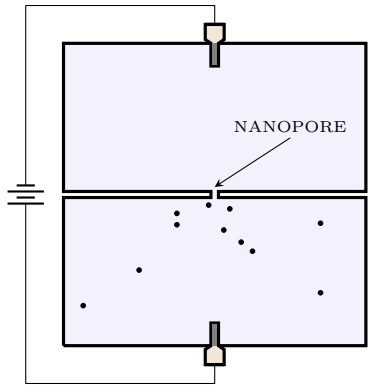


FIGURE 3.1. Cross-section of a conventional nanopore experimental apparatus.

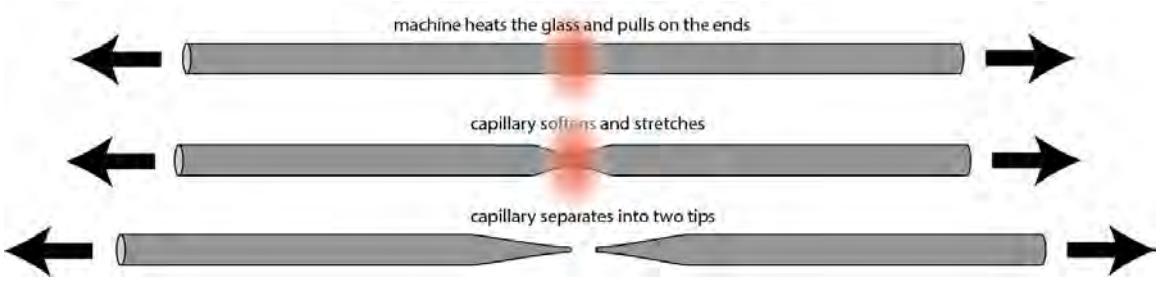


FIGURE 3.2. Schematic of a glass capillary being heated and pulled by a micropipette puller to produce two extended solid-state nanopores, which can then be imaged and used in experiments.

that measure 0.3–0.7-mm inner diameter and 1-mm outer diameter, which taper to a nanopore tip at one end. The exact length and diameter of the overall capillary depends on the initial capillary used; both the capillary used and the settings with which the capillary was pulled influence the shape and size of the nanopore created.

We fabricate nanopores from borosilicate and quartz capillaries to create a wide range of tip diameters and various lengths and taper angles. For quartz capillaries, which are stronger and more stable than borosilicate capillaries in smaller sizes, we have designed recipes that consistently yield diameters of 40–60 nm and 1–5 $\mu$m in length. For borosilicate capillaries, for which we have easier access to an appropriate pipette puller but are not as stable as quartz at smaller tip diameters, we have designed recipes that yield tip diameters of 70–120 nm and lengths comparable to those of the quartz capillaries. As can be seen in Fig. 3.3, borosilicate tips generally have longer tapers than quartz tips.

Fabrication by heating and pulling capillaries requires a high level of control over both processes, in much the same way as a high level of precision is required to drill a nanopore of a given size electrically. Using pipette pullers from Sutter Instruments, the Stein lab is able to control all four parameters above—heat, duration, force, velocity—as well as pressure in the pipette puller. For borosilicate capillaries, the P-97 Micropipette Puller is used. However, since quartz has stronger thermal properties, the P-2000 Laser-Based

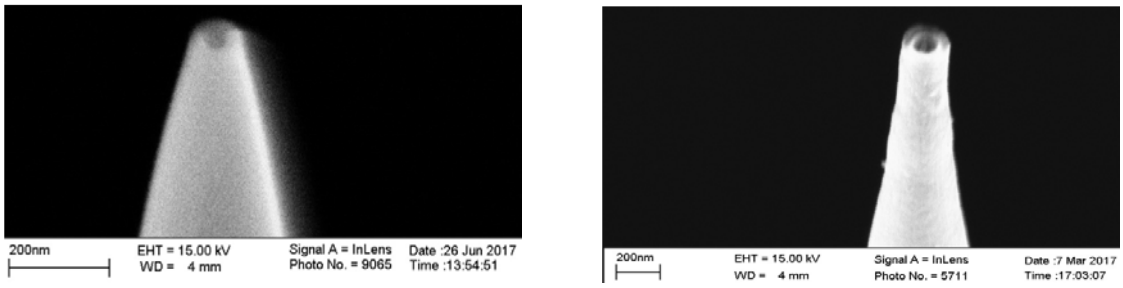


(A) 45-nm inner diameter quartz tip. (B) 100-nm inner diameter borosilicate tip.

FIGURE 3.3. Scanning electron micrographs of solid-state nanopores from different used in experiments. Stronger quartz capillaries are more stable in smaller inner diameters and have shorter tapers; borosilicate capillaries are easier to fabricate, offering a different advantage.

Micropipette Puller is required, as filament, heat-based pullers are not powerful enough to stably fabricate quartz capillaries.

Once fabricated, capillary tips are coated with a 5-nm layer of carbon using a carbon thread evaporator, and then they are imaged in a scanning electron microscope before being used in experiments. The carbon coating allows them to be visible in the electron microscope. Through imaging, we are able to determine the precise inner diameter, length, and taper of each tip, allowing us to predict translocation duration, frequency, and signal strength; imaging also allows us to determine whether the nanopore tip is patent, since obstructions would naturally prevent translocations. After fabrication and imaging, a capillary is plasma cleaned on room air for three minutes before use in experiments. Plasma cleaning increases the hydrophilicity of the inner surface of the nanopore.

## 2. Fluidic Cell

The first experiments we conducted were run in a fluidic cell already in use by the Stein Lab for other experiments. This cell simply held two chambers of solution, connected them with the same type of capillary nanopore we use to detect John Cunningham Virus translocations, and screw holes for electrodes and a pressure insert; essentially, it was Fig. 3.1 with a capillary. However, to use the pressure insert required forcing air directly into the fluidic cell, resulting in the introduction of air bubbles to the apparatus. Once these bubbles reached the nanopore, they made translocations impossible to detect and ended the experiment. Additionally, the mechanism that sealed the nanopore to the fluidic cell was not always tight, and occasionally a leak could occur which allowed fluid (and virus particles) to diffuse between chambers without translocating through the pore. These leaks short the electrical circuit we want to monitor and have to be sealed properly for experiments to work.

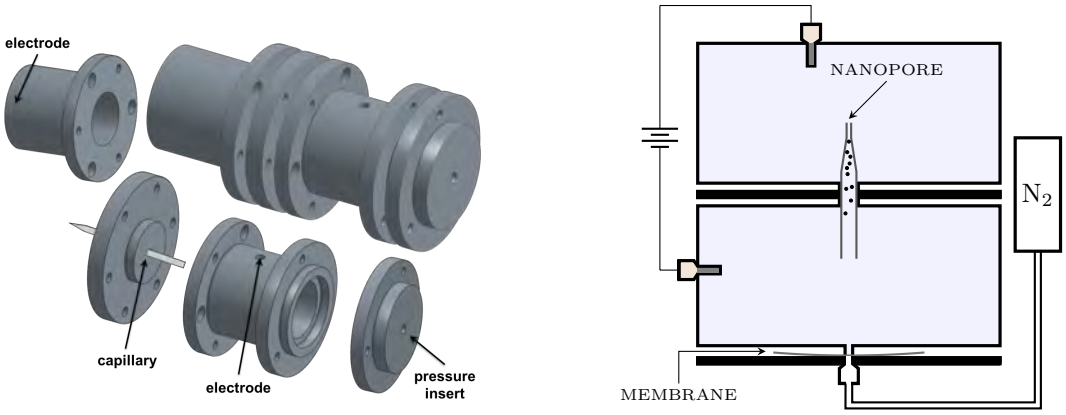


(A) Different pieces of the fluidic cell. (B) Cross-section of our modified fluidic cell.

FIGURE 3.4. Design of the fluidic cell that houses salt solution, pore, viruses, and inserts for electrodes and tubing to apply electric fields and pressure gradients. A membranous material between the two rightmost pieces of the cell above allows for application of a pressure gradient, but no introduction of microscopic air bubbles into the apparatus.

To improve our control over the variables that determine the duration and signal strength of virus translocations, we designed and built a unique fluidic cell for this experiment. The cell is capable of simultaneously controlling the applied voltage and pressure gradient that promote translocations of the John Cunningham Virus. With the new cell, application of a pressure gradient does not actually introduce any air into the fluidic cell, and the fit of the nanopore is improved so that interchamber leaks are much rarer.

Fig. 3.4a shows the different parts to the fluidic cell, whereas Fig. 3.4b depicts a schematic of a cross-section of the assembled apparatus. The two main compartments of the fluidic cell house the two salt solutions as well as the electrode inserts. Between them is a piece that stabilizes the 4–5-cm capillary. The two main chambers are screwed onto either side of the middle piece, and O-rings on either side seal the two chambers. On one side—in our experiments, the side with the widened end of the capillary, as in Fig. 3.4a—a membranous material separates the main piece from the cap. By inserting this membranous material, application of a pressure gradient—which is done by connecting the fluidic cell to the line of a gas tank—does not push air into the fluidic cell or nanopore. Air bubbles in the nanopore can be difficult to remove, make it difficult or impossible for virus particles to translocate, and usually require the apparatus to be disassembled and refilled before the experiment can be re-run. Alleviation of that problem is one of the key features that makes this fluidic cell superior to alternatives for our experiments.

## 3. Setup and Experimental Methods

Running a conventional nanopore experiment occurs in several stages. First, the nanopore must be fabricated and imaged to determine its precise geometry. Then the apparatus needs to be assembled, as it is in Fig. 3.1 with two chambers of salt solution bridged only be the nanopore. Before adding biomoleculces,

the system's baseline current is tested; electrodes are connected to either end of the apparatus and an electric potential difference is applied; the voltage is varied over a range of values, and the mean value of the current is taken at each of those values; the results are plotted on an IV curve. If the baseline current is stable and within an order of magnitude of estimates, and if the IV curve shows agreement with Ohm's Law with a reasonable effective resistance, then the apparatus is disconnected from the power source and the biomolecules to be translocated are added to one of the chambers. If these required conditions are not obeyed, the cell is disassembled and re-assembled in attempt to fix the errors. Once biomolecules are immersed in one of the chambers, the electric field is reapplied, and the current across the pore is monitored for translocation signals.

To begin an experiment, all fluidic cell components and the syringes and needles used to add fluid and virus particles to the fluidic cell are rinsed out with deionized water. Both electrodes are scraped clean of any precipitate from the previous reaction, rinsed with deionized water, and submerged in bleach for twenty minutes away from any light sources; then they are rinsed clean again with deionized water. The salt solution to be used is bath sonicated for ten minutes to ensure all ions are dissolved and uniformly diffused.

The capillary nanopore, after being plasma-cleaned for three minutes, is inserted into the appropriate piece of the fluidic cell, and it is filled with salt solution. After being filled with solution, the capillary is viewd under an optical microscope to check for microscopic air bubbles that might prevent results. The surrounding chambers are attached, filled with solution, and the cell is sealed. At this point, baseline tests are performed.

Assuming the IV curve shows a linear shape with a reasonable slope, and that the baseline current is stable, the apparatus is disassembled, and virus particles are injected inside the capillary directly proximal to the tapering tip. Then the fluidic cell is re-assembled, and the electrodes and pressure tubing are connected. The fluidic cell is placed in a Faraday cage, which minimizes external electrical noise.

In experiments, current is measured by connecting the electrodes of the fluidic cell to an AxoPatch device specifically designed to detect current at the scale of pA. A 50-kHz filter in the analog current-to-voltage amplifier sets the bandwidth limit of the technology and therefore how quickly the John Cunningham Virus particles can pass through and still be accurately detected: 20 $\mu$s. The expected durations from the theory in Ch. 2 are barely large enough to allow for these virus particles to be detected using our apparatus.

## 4. Diagnostic Tests of Experimental Apparatus

After building the new fluidic cell, we needed to run diagnostic tests similar to those run at the beginning of each individual experiment to make sure the apparatus worked well. By gauging the response of the apparatus to variations in applied voltage and applied pressure, as well as the deviation of the current over time when no parameters change, we can characterize the stability of the apparatus. Ideally, our theory

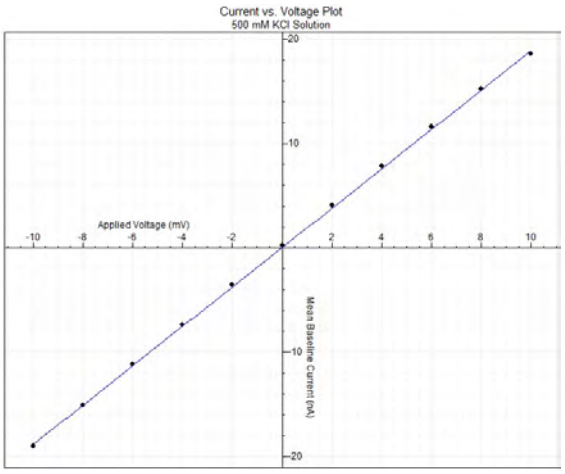


(A) Current vs. Voltage curve shwoing Ohmic behavior of nanopore sensor. Data follows a linear fit with correlation coefficient $r = 0.983$.

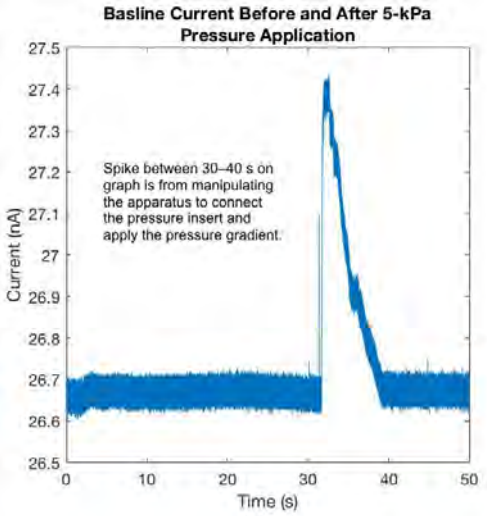


(B) Plot of current vs. time before and after a 12-kPa external pressure was applied on top of a 300-mV voltage difference across 150-nm borosilicate nanopore immersed in 1 M KCl solution. Resultant streaming current $i = 91.6\,\text{pA}$.

FIGURE 3.5. Tests of fluidic cell's ability to measure electrical current show a stable dependence on applied voltage and a negligible dependence on applied pressure, as expected from the theory in Ch. 2.

suggests we should see a linear dependence of current on applied voltage, a minimal change upon application of an external pressure, and a steady baseline current if the apparatus is left alone.

Before testing the apparatus's capability to detect translocations of the John Cunningham Virus, to ensure that the fluidic cell stably housed a nanopore, we first ran experiments to ensure that the current increased linearly with voltage, obeying Ohm's law as required. Plots of average current against applied voltage revealed the linear relationship for capillaries whose nanopore tips had not broken during insertion into the apparatus; an example of an IV curve is shown in Fig. 3.5a. Furthermore, we determined that the constant of proportionality depended appropriately on the measured conductivity of the salt solution used in the experiment. In the example in Fig. 3.5a, $R_0 = 5\,\text{M}\Omega$, a reasonable estimate for our pore geometry and salt concentration.

After making the determination that the cell was stable in response to changing electrical potential, we monitored how the current changed under application of varying pressure gradients; the baseline current showed no modification before versus after application of a pressure gradient across the pore. This result was in agreement with the prediction of Eq. (2.16) that the streaming current from application of a pressure gradient should be more than an order of magnitude lower than the baseline current created by the electric field across the nanopore. This result can be seen in Fig. 3.5b. There, the streaming current can be calculated based on the difference between the mean current before and after the pressure gradient was applied. This

method gives a streaming current of $i = 91.6\,\text{pA}$ against a baseline current of $I_0 = 26.7\,\text{nA} = 290i$, justifying our being able to ignore the effects of streaming current with this apparatus.

Baseline current measurements showed that in roughly half the experiments run, the value of the baseline current would drift slowly, at rates as high as $5\,\text{nA/min}$. These minor variations in baseline current over time are not concerning in regard to the stability of the apparatus in measuring electricl current, and a small amount of change in baseline is inevitable in experiments this sensitive. Our observed drifts are often linear and over a long period of time, and can therefore be easily accommodated for by means of a baseline correction in the final graph of current vs. time. Such a modification is easy to make in Clampfit, the software that analyzes data collected by the Axopatch technology.

Completion of these baseline tests indicates that our newly-designed apparatus is capable of stably monitoring current at the scale of nA and pA, which is what our experiments will ultimately require.

CHAPTER 4

# Electrical Measurements of Synthetic and Biological Nanoparticles

The ultimate goal of developing this refined apparatus is to detect the translocations of the John Cunningham Virus through solid-state nanopores. To do that, after we designed built our new fluidic cell, we tested it first without any spherical particles—the results of which are shown in Fig. 3.5—then with silica nanospheres as diagnostic tools, and then finally with John Cunningham Virus particles.

Most of the results we analyze from these experiments come in the form of graphs of current vs. time. From these graphs, we are able to obtain the duration, intensity, and frequency of translocations. By analyzing how those variables vary under different virus concentrations, voltages, pressures, and solution conductivities, we determine how confidently we can assume that the current spikes observed are, in fact, from virus translocations and not the result of another, unaccounted for, phenomenon such as noise.

## 1. Silica Nanosphere Diagnostic Experiments

After determiming the stability of the fluidic cell, we tested our apparatus on silica nanospheres of varying diameters: 20 nm, 50 nm, and 100 nm. We tested these spheres using roughly the same concentrations as our samples of the John Cunningham Virus: $3 \times 10^8$ particles/mL. Since these viruses come in the approximate size and shape of the John Cunningham Virus, a sensor that can detect translocations of silica nanospheres should also detect translocations of John Cunningham Viruses.

We suspended the nanospheres in a basic solution of 500 mM KCl with 10 mM Tris base, titrated to pH 9.0 using concentrated potassium hydroxide and hydrochloric acid solutions. Particularly for silica surfaces, a basic environment allows for deprotonation of the silanol groups on the surface of the glass, exposing a negative charge on both the spheres and the nanopore surfaces. These negative charges prevent clumping of nanospheres to each other, which would make them too large to translocate through the pore; the basic environment also prevents the spheres from adhering to the surface of the nanopore.

Detection of 100-nm nanospheres—our sample of which actually contained nanospheres of average diameter $110 \pm 4$ nm [14]—requires a larger borosilicate pore, since a pore smaller in diameter than the virus will not allow for any translocations. Therefore, the capillary used that ultimately detected these translocations was a 150-nm borosilicate capillary with a considerably longer length than other pores used, its length on the order of 1 $\mu$m. We used 1 M KCl and 10 mM Tris base solution, titrated to pH 9.0, and applied a 300-mV potential difference and a 12-kPa pressure difference across the pore. Because of the nanopore's increased

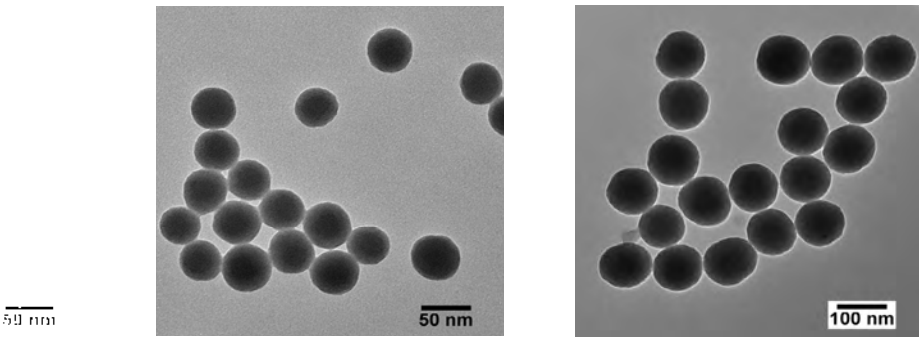


(A) 20-nm Nanospheres [15]. (B) 50-nm Nanospheres [16]. (C) 100-nm Nanospheres [14].

FIGURE 4.1. Scanning Electron Micrographs of different size nanospheres used in diagnostic experiments to test our nanopore sensor.

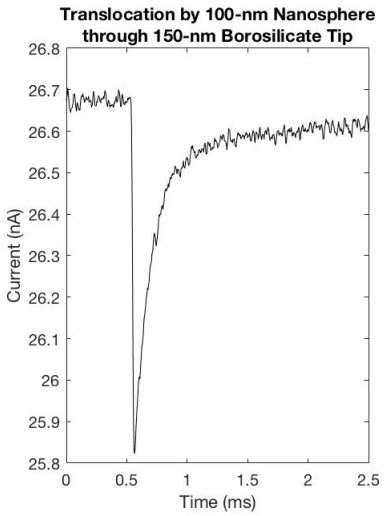


FIGURE 4.2. Translocation of 100-nm nanosphere through 150-nm diameter, 1-$\mu$m-long, borosilicate capillary. Applied voltage of 300 mV; applied pressure 12 kPa; Solution is mM KCl, 10 mM Tris, and titrated to pH 9.0.

length, the translocation times of the 100-nm nanospheres were considerably longer. An example of one translocation is given in Fig. 4.2. It should be noted, however, we did not detect many other translocations of 100-nm nanospheres.

A unique feature of the 100-nm translocation is that the shape of the signal on the current vs. time chart provides insight into how that nanosphere translocated. Whereas the spheres are injected into the apparatus just proximal to the tip of the capillary, some do diffuse through to the far chamber before we start measuring current. If the electric field and pressure gradient are applied in a certain direction, a nanosphere could be pushed back through the tip and up through the taper. Such a translocation would appear as a sudden drop in current followed by a gradual rise back to baseline, the taper angle responsible for the gradual return. This shape is exactly the shape of the translocation seen in Fig. 4.2.

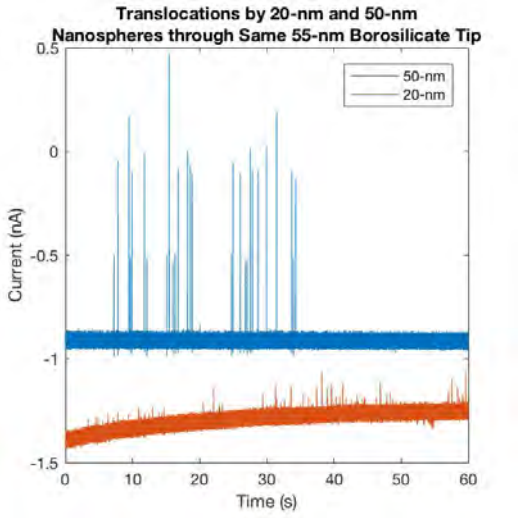


(A) Full-scale current vs. time plot of 20-nm and 50-nm nanosphere translocations.

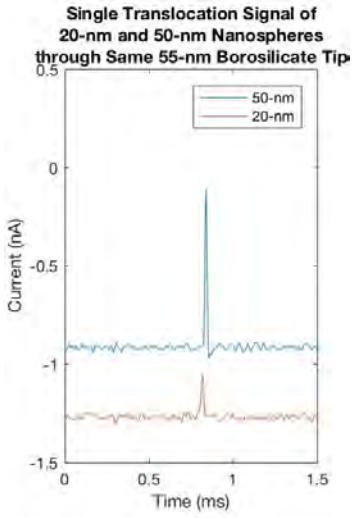


(B) Zoomed view of a single translocation for 20-nm and 50-nm nanosphere translocations.

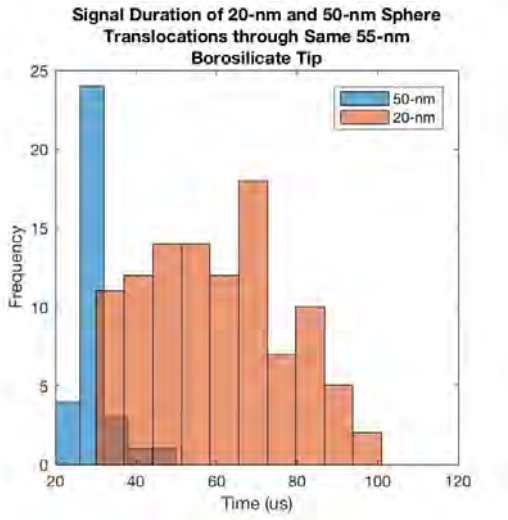


(C) Histogram of translocation signal durations for 20-nm and 50-nm nanospheres. Average durations with standard deviation of mean are $\Delta t_{20} = 59.9 \pm 1.7\,\mu$s and $\Delta t_{50} = 29.2 \pm 0.8\mu$s.

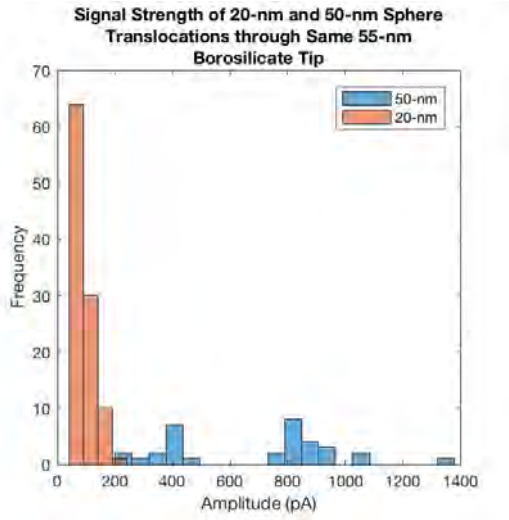


(D) Histogram of translocation signal amplitudes for 20-nm and 50-nm nanospheres. Average amplitudes with standard deviation of mean are $\Delta I_{20} = 90.9 \pm 3.4\,$pA and $\Delta I_{50} = 679.6 \pm 49.8\,$pA.

FIGURE 4.3. Collected data for 20-nm and 50-nm nanosphere translocations through the same 55-nm borosilicate tip. Particle concentration $3 \times 10^8$ particles/mL submerged in 500 mM KCl, 10 mM Tris, pH 9.0. 50 mV applied voltage; no pressure gradient.

Experiments for translocations of 20-nm and 50-nm diameter nanospheres—whose actual average diameters for our samples were $21.4 \pm 2.7$ nm [15] and $47 \pm 3$ nm [16], respectively—were run using a 55-nm borosilicate capillary tip, this tip of length 100 nm, yielding translocation times that were much shorter. These experiments were run in 500 mM KCl, 10 mM Tris base, titrated to pH 9.0, and were under the influence of a 50-mV potential difference and no pressure gradient.

The results of the 20-nm and 50-nm nanosphere translocations are depicted in Fig. 4.3. The histograms in Fig. 4.3c–4.3d show a clear distinction between the translocation times of the two different sizes, though the variation in duration is much larger for the 20-nm nanospheres than it is for the 50-nm nanospheres. The signal strength for the 50-nm nanospheres is almost as large as the baseline current at times, while the signal strength for the 20-nm nanospheres is 13% that of the 50-nm spheres. Intriguingly, the distribution of signal strengths for the 50-nm spheres is bimodal.

From the translocations detected for 20-nm, 50-nm, and 100-nm silica nanospheres and the previous baseline current measurements show encouraging evidence that our nanopore sensor is capable of detecting translocations of spherical particles, and that it can be applied to detect translocations of the John Cunningham Virus.

## 2. John Cunningham Virus Translocations

Translocations of the John Cunningham Virus through a 60-nm quartz capillary are shown in Fig. 4.4–4.5. For these experiments, a slightly basic solution of the same composition as that used to test the 20-nm and 50-nm nanospheres was used, since it was successful for those and since a basic solution will also successfully deprotonate the polar head groups on the virus membrane. This deprotonation, like that on the silanol surface of the nanospheres, creates a greater negative charge density on the surface of the viruses (albeit not as much as the charge density created on the silica spheres); charged virus particles are more responsive to an electric field and less likely to adhere to neighboring viruses or the negatively-charged nanopore surface.

Translocation graphs are shown in Fig. 4.4 for four different circumstances. In the baseline condition, virus particles were inserted into the apparatus at a concentration of $3 \times 10^8$ virus/mL; a 10 mV potential difference was applied without a pressure gradient. We then performed three follow-up experiments, each making one change to the apparatus from the baseline condition; the current was monitored again for translocations. In one follow-up trial, we doubled the voltage to 20 mV; in another, we applied a 5-kPa pressure gradient; in the final, we flushed out the capillary with excess salt solution and re-introduced virus particles at half the initial concentration ($1.5 \times 10^8$ virus/mL).

When the voltage was doubled, the baseline current approximately doubled as well, and other parameters changed slightly as can be seen in the Histograms in Fig. 4.5b–4.5d. The average signal intensity increased ($p = 3 \times 10^{-4}$), and the average time between signals decreased ($p = 0.02$). These events also showed a statistically significant difference in mean signal duration ($p = 0.05$), though the difference was only 5 $\mu$s.

When a 5 kPa pressure difference was applied across the cell with all other conditions equivalent to baseline, the current vs. time graph for which is depicted in Fig. 4.4c, the signal intensity increased as well ($p = 0.01$). Interestingly, when the pressure was doubled to 10 kPa, which happened at $t = 30$ s in Fig. 4.4c, all event signals disappeared.

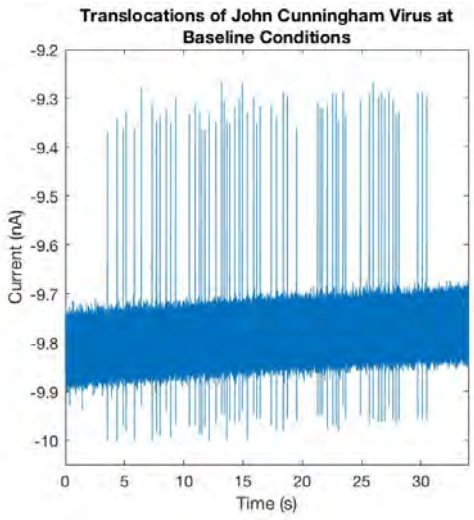


(A) Baseline conditions.

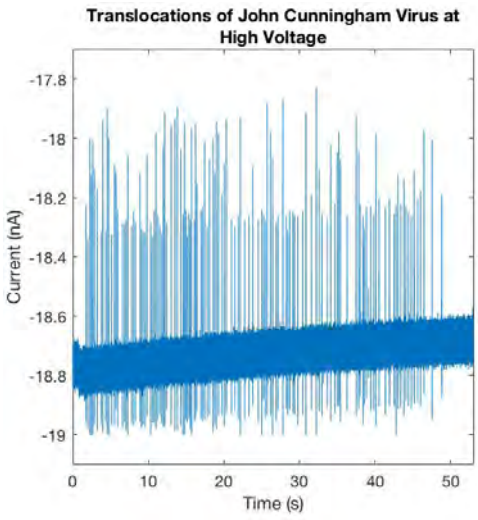


(B) High-Voltage (20 mV).

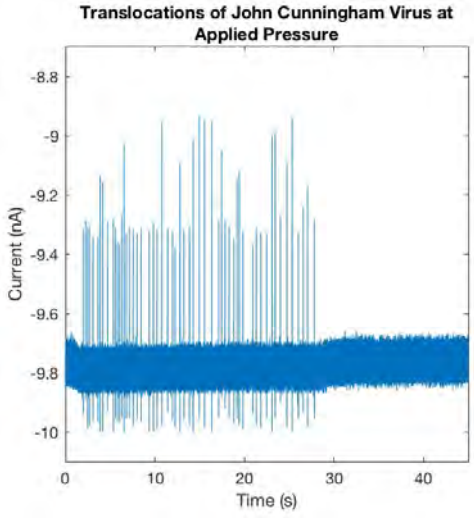


(C) 5 kPa applied pressure, doubled to 10 kPa at 30 s.

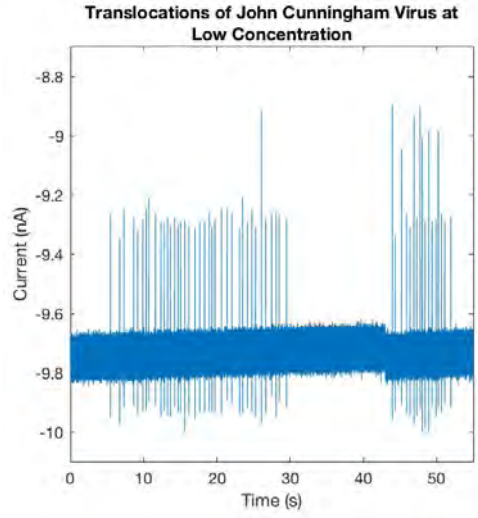


(D) Low Concentration ($1.5 \times 10^8$ virus/mL).

FIGURE 4.4. Current vs. time graphs for John Cunningham Virus translocations through a 60-nm quartz capillary tip. At baseline conditions, the applied voltage is 10 mV, there is no pressure gradient, and the particle concentration is $3 \times 10^8$ virus/mL. Virus particles immersed in 500 mM KCl, 10 mM Tris base, titrated to pH 9.0.

A decrease in concentration showed a statistically significant change in mean event duration ($p = 0.04$), though this difference is even smaller than that resulting from doubling the voltage: 2 $\mu$s difference from baseline. The halved concentration also increased the average time between translocations ($p = 0.02$). The current vs. time plot for this experiment showed a lull of approximately 12 s between two shorter intervals of frequent electrical events. Note that no statistical difference can be observed between the two temporal regions of events.

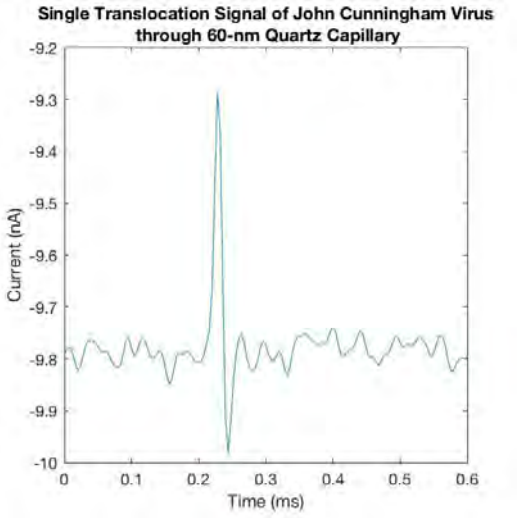


(A) Zoomed-in view of a single translocation of a John Cunningham Virus through 60-nm quartz capillary tip under baseline conditions (10 mV; 500 mM KCl, 10 mM Tris, pH 9; $3 \times 10^8$ virus/mL).

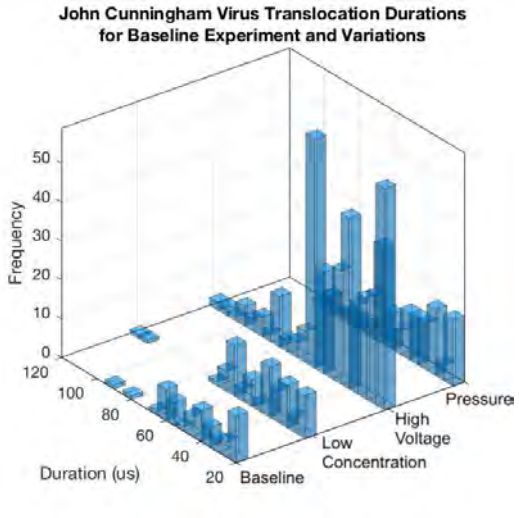


(B) Histogram of translocation durations. Baseline mean of 43 $\mu$s; high-voltage mean of 48 $\mu$s ($p = 0.05$); applied pressure mean of 48 $\mu$s ($p = 0.08$); low-concentration mean of 45 $\mu$s ($p = 0.44$).

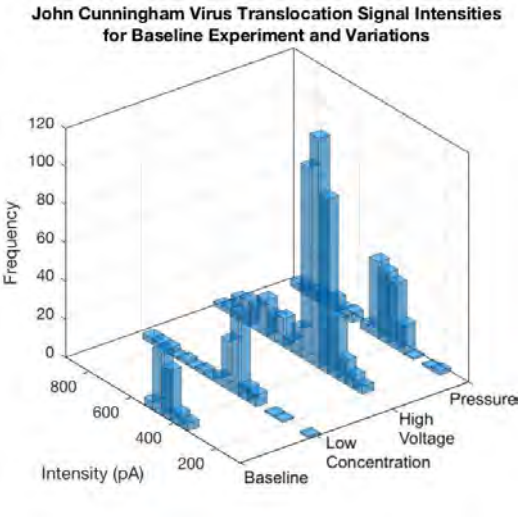


(C) Histogram of signal intensities. Baseline mean of 456 pA; high-voltage mean of 482 pA ($p = 3 \times 10^{-4}$); applied pressure mean of 485 pA ($p = 0.01$); low-concentration mean of 483 pA ($p = 0.04$).

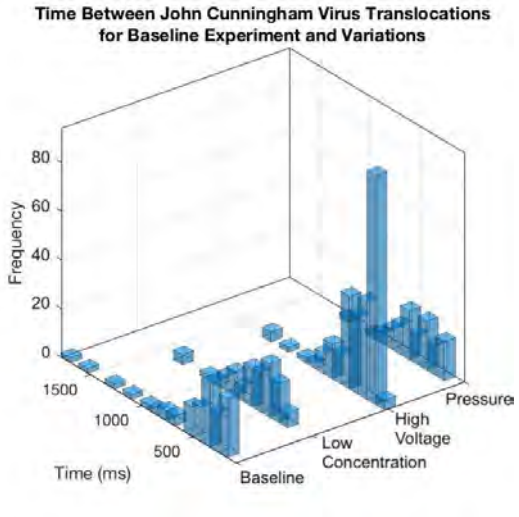


(D) Histogram of time between translocations. Baseline mean of 480 ms; high-voltage mean of 367 ms ($p = 0.02$); applied pressure mean of 477 ms ($p = 0.94$); low-concentration mean of 604 ms ($p = 0.02$).

FIGURE 4.5. Translocation data from current vs. time plots in Fig. 4.4. Histograms and shapes of individual signals included. Each histogram is captioned with the mean values of the variable under all four conditions, along with a $p$-value indicating whether any change from the baseline condition is statistically significant.

CHAPTER 5

# Analysis of Electrical Events

Unlike experiments that can be monitored visually under a microscope, in these nanopore experiments it is not possible to directly visualize the nanopore during virus translocations. Therefore, the determination that an electrical event is the result of a translocation can only be a prediction. By analyzing the shapes of the signals, the circumstances in which they appear, and how they respond to variations of the parameters of the experiment, we can develop a level of confidence—or lack thereof—that the signals are, in fact, indicators of virus translocation events.

For example, large spikes in of themselves do not indicate virus translocations if the spikes are equally likely to occur in either direction with the same magnitude; those signals are indicative of external electrical noise. Signals that are interspersed at perfectly regular intervals with minimal deviation in time between translocations are unlikely to be virus translocations, since a virus's motion is mostly random, particularly before it reaches the nanopore. Naturally, if signals of the same shape occur both with and without virus particles suspended inside the capillary, they are responding to an event other than a virus translocation.

To some degree, we expect the duration, intensity, and frequency of translocations to change upon variations of different parameters of the experiment. Frequency should increase with increasing concentration, since a higher concentration implies more closely-packed virus particles; when more particles occupy the same space, it is more likely that one will undergo a random walk into the nanopore at any given time, at which point the electric field and pressure gradient guide it through the pore. Signal intensity should increase with increasing voltage—as should baseline current—according to Ohm's Law, because a change in current is proportional to the applied voltage in either the high or low conductivity models, according to Eq. (2.14). A change in pressure or a change in voltage should change the duration of translocation, since the velocity of the virus is dependent on these properties.

For the 20-nm and 50-nm sililca nanosphere data and the data for the John Cunningham Virus trials, we analyze these three output variables, and determine if they change according to our theory as we vary the parameters over different experimental trials. Our results show some promising evidence that we are detecting translocations, while leaving other unexpected results unanswered and in need of further investigation.

### 1. 20-nm and 50-nm Silica Nanosphere Data

The signals from the experiments run on the 20-nm and 50-nm nanospheres in Fig. 4.3 suggest that they may be the result of translocations. The size of the signals varied significantly between the trial with 50-nm nanospheres submerged and the trial with 20-nm nanospheres submerged, with the signals in the 20-nm trial roughly 13% the size of the 50-nm signal. According to Eq. (2.12), the 20-nm signals should be 6% that of their 50-nm counterparts if these signals are truly detecting translocations. The close resemblance of the results to the predictions of the Resistive Pulse Technique lends credibility to these events being nanosphere translocations. Reasonably, the 50-nm nanospheres' signals are almost as large as the baseline current, as should be expected if a 50-nm diameter resistive particle occludes a 55-nm diameter pore.

The translocation durations of the nanospheres also provides relatively convincing evidence that these signals are, in fact, translocations. As explained in Ch. 2, for the lengths of nanopores we use, diffusive effects are negligible compared to electrokinetic effects in determining translocation duration; therefore, when no pressure gradient is applied, the translocation duration is determined largely by electrokinetics. From that observation, we can assume that a particle with a larger electrokinetic ($\zeta$) potential will translocate more quickly. In our experiments, the 20-nm nanospheres had an average duration twice as large as that of their 50-nm counterparts; when analyzing the $\zeta$ potentials of these particles as experimentally determined by the supplying company, the electrokinetic potentials were $\zeta_{20} = -31\,\mathrm{mV}$ and $\zeta_{50} = -51\,\mathrm{mV}$ [15, 16]. For a near doubling of electrokinetic potential, we observed signals half as long. Furthermore, the durations themselves are also on the same order of magnitude as the predictions of the theory: between 20–100 $\mu$s.

Given that both the signal intensity and duration of the 20-nm and 50-nm nanosphere trials varied in a manner that conformed closely to how our theory predicts translocation signals should behave, we can develop a sense of confidence that these signals were, in fact, the result of nanosphere translocations, which supports the conclusion that our fluidic cell has the potential to detect John Cunningham Virus translocations.

### 2. Analysis of John Cunningham Virus Experiments

The four trials of translocating John Cunningham Virus particles through a 60-nm quartz capillary, the results of which are outlined in Fig. 4.4–4.5, all produced signals of a relatively similar shape. Many features of these signals, particularly the means by which they vary on the different parameters of the experiment, offer fairly convincing evidence that they are, in fact, indicators of John Cunningham Virus translocations. Other observations about the shapes of these signals, along with the consistency of experiments that yield results such as those shown in the relevant figures bring into question whether these signals adhere to our expectations of translocation signals.

The nature of our experimental data for John Cunningham Virus trials allows us to compare several different experiments to a single baseline experiment: an increase in voltage, an application of a pressure gradient, and a decrease in concentration. This structure allows us to analyze how the duration, intensity, and frequency—or in our case, its conjugate variable, the time between translocations—vary when we manipulate a single parameter. For each of these variations, we analyze whether there is a statistically significant difference for each of the three analyzed variables, and whether that difference is large enough to actually be considered a true change.

**2.1. Variation of Translocation Duration.** The average baseline signal duration of $43\,\mu$s increased to $48\,\mu$s ($p = 0.05$) under a high voltage. While these results are statistically significant, they are likely negligible. A doubling of a voltage resulting in a 10% increase in translocation time is nonsensical; the change in duration should not only be proportional to the change in voltage, but it should decrease with an increase in voltage. This result is, therefore, while statistically significant, likely not scientifically significant.

Analysis of signal duration is complicated in this particular case. If a doubling of the potential difference halved the duration of signals as we would expect it to, then the mean translocation time would be approximately $20\,\mu$s; roughly 50% of translocations would be less than that time, undetectable after being filtered out by our electronics. Because the translocation durations of our virus particles lie at the very lowest limit of our electronics' bandwidth, measuring changes in these durations can be extraordinarily tricky and cannot always be expected to yield the results our theory predicts.

This observation about the relationship of translocation duration and our apparatus's bandwidth potentially sheds light on why signals during the applied pressure trial stopped after the pressure was doubled to 10 kPa. The application of a pressure gradient in combination with an applied voltage should increase the translocation velocity of the virus particles, according to Eq. (2.3). Further increasing the pressure gradient could very well increase that translocation velocity beyond the critical speed corresponding to the lower limit of our electronics equipment. The translocations may still be occurring, but our apparatus is unable to detect them.

**2.2. Variations of Signal Intensities.** Intensity of the signals increased from baseline in all three subsequent experiments: high voltage ($p = 3 \times 10^{-4}$), applied pressure ($p = 0.01$), and decreased concentration ($p = 0.04$). In all three cases, the change was to approximately 480 pA from 450 pA. The fact that the change was the same in all three of these variations indicates that the change itself might be due to an unintentional change in the apparatus created while reassembling the fluidic cell.

Much like duration of translocations is difficult to rely on for these data due to how short the signals are, the value of the intensity is difficult to rely on. There are not enough data points on a single translocation for us to ensure that the peak recorded on the current vs. time graph is reflective of the actual amouunt by

which a virus particle decreased the amplitude of the electrical current. Given this fact, while our theory expects that increasing voltage should increase the mean signal intensity, it is not surprising that an increase in the applied voltage does not cause a comparable increase in signal strength of the events on the plots of current versus time.

In light of this caveat, comparing Fig. 4.4b to Fig. 4.4a, we observe that despite the lack of change in average intensity, there are a significant number of peaks in Fig. 4.4b that are nearly twice as large as those in Fig. 4.4a: upwards of 1 nA as opposed to 400–500 pA. These larger peaks in Fig. 4.4b may be reflective of translocations whose peak signal was more accurately measured by the Axopatch software. Based on this observation, the results of the trial run at high voltage offers potential evidence that these electrical signals may be reflective of virus translocations.

**2.3. Analysis of Time Between Signal.** Compared to the mean baseline lapse between consecutive events of 480 ms, the experiment with doubled applied voltage had a smaller mean lapse of 367 ms ($p = 0.02$), and the experiment with a decreaased concentration had a greater mean lapse of approximately 600 ms ($p = 0.02$). The application of a pressure gradient created no change in mean lapse whatsoever ($p = 0.94$). After reconciling these observations, they all support the notion that these signals are detections of John Cunningham Virus translocations.

Decreasing the concentration should certainly decrease the frequency of translocations. In the decreased concentration trial, whose result is shown in Fig. 4.4d, a halved concentration resulted in a 30% increase in time between events, indicating a responsiveness of output electrical signals to changing concentrations; such an observation supports the notion that the signals represent translocations.

The effects of increasing the potential difference (and electric field) across the pore on translocation frequency make sense when considering the shape of capillary nanopores. Unlike conventional membrane nanopores, capillary nanopores taper gradually to a tip. Therefore, since the electric field varies inversely as $E \propto r^{-1}$, it is not negligible in the space proximal to the nanopore. The presence of an electric field in this region would guide virus particles toward the pore. An increase in the strength of the electric field should guide virus particles toward the pore more quickly, thus explaining the decreased lapse between consecutive events observed under conditions of increased voltage. This theoretical explanation for the observation that an increased electric field yields a decrease in time between electrical signals lends additional credibility to the potential for these events to be virus translocations.

While the electric field varies inversely as the pore size, in a Poiseuille Flow, the pressure gradient varies as $\nabla p \propto r^{-4}$, so the pressure drop is entirely across the nanopore. Therefore, the effects of Poiseuille flow will not be relevant outside the nanopore, and the application of a pressure gradient will not play a role in guiding virus particles toward the capillary tip. We should not expect the frequency of translocations to

increase. Therefore, the lack of change under application of a 5 kPa pressure gradient should be encouraging that signals are only responding to the correct variables.

The lapse between measured electrical signals strongly lends credibility to the potential for those signals to represent John Cunningham Virus translocations. The output variable is responsive to virus concentration and applied voltage, the parameters that should have a significant influence on it, but does not change when we vary the applied pressure, a mostly unrelated parameter to this particular output.

**2.4. Areas of Concern.** While analysis of the observed signals' variation with the changes to experimental parameters offer support to the signals' being evidence of virus translocations, the data are not perfect. Analysis of Fig. 4.5a shows a single translocation event, which is typical of most others in the plots in Fig. 4.4. After the initial decrease in current amplitude, before returning to baseline the current forms a peak in the opposite direction, approximately 25% of the initial peak. While this secondary peak is not the same amplitude as the primary signal, it may be too large to be considered negligible, and virus translocations should not create such a rebound spike in the opposite direction. This shape of the signal is difficult to interpret, and may be the result of the Axopatch software's difficulty in creating the exact profile of current versus time on such short time scales.

Another concern is that electrical event signals are not always detectable each time the apparatus is assembled. Some experiments—like that for the 100-nm nanospheres in Fig. 4.2—detect one or two translocations; others—like those depicted in Fig. 4.3 for the 20-nm and 50-nm nanospheres and in Fig. 4.4–4.5 for the John Cunningham Virus—detect numerous translocations; and yet others detect none regardless of time spent monitoring the electrical current. Often times, the capillaries that work extraordinarily well once work just as well in future experiments, as is evidenced by the use of the 55-nm borosilicate and 60-nm quartz capillaries for the main experiments in this section; the capillaries that do not work at all in one experiment never yield translocations, likely due to a poor fabrication that led to a nanopore that was not fully patent. Often however, simply disassembling and reassembling the apparatus can help an experiment that wasn't detecting virus previously work better.

The fact that experiments are not always reproducible offers additional cause for concern, but this concern has less to do with whether the signals we observe are indeed virus translocations, and more to do with whether we completely understand the experimental setup that allows us to detect those virus translocations. Proper assembly of the fluidic cell requires introduction of virus particles close enough to the tip that they will diffuse to the nanopore in a reasonable time frame. Additionally, no microscopic air bubbles can be introduced into the system, which could happen during insertion of virus particles as well as during sealing of the fluidic cell. Where the setup goes awry in experiments that fail to detect any virus translocations remains unknown at this point.

The data presented in Ch. 4 and analyzed in this chapter for experiments testing synthetic and biological molecules show a promising potential for our apparatus to expand the uses of nanopore sensors to detect smaller, spherical biomolecules like the John Cunningham Virus.

CHAPTER 6

# Conclusions

Monitoring electric current across nanopores as a technique of detecting single biomolecules originated in an attempt to detect DNA polymers, which are long and filamentous in shape. The optimization of nanopore sensors to detect translocations of spherical viruses offers the potential to expand the types of biomolecules detectable using this technology. However, without slowing down the virus particles and extending the duration of translocations, the translocations of particles less than 100 nm in diameter are too short to be detected by most modern technologies. This project has aimed to solve that problem by extending the lengths of the nanopores used and designing a fluidic cell capable of more precise control over the parameters that promote virus translocations, in hopes of detecting translocations of the John Cunningham Virus through solid-state nanopores.

By using a different type of nanopore, we fabricated pores long enough to accommodate the smaller size of spherical virus particles. The data we cikkected for synthetic and biological particles suggest that their translocations are detectable by our extended capillary nanopores. The properties of the electrical signals are responsive to changes of the appropriate parameters, and they are only present when the virus particles are introduced into the apparatus. Under a small electric field and pressure gradient, we slowed the virus translocations so their signals were not filtered out by the electronics equipment.

Future experimentation for this research will have to address the lack of consistency of these experiments in detecting virus translocations, which will likely require developing a better method of guiding virus particles toward the nanopore in a controlled manner. Another goal should be to further slow down the virus particles during translocation and allow the nanoelectronics technology to acquire more data points for each translocation, more data points corresponding to more information about each translocation. Slowing down the virus particles by an additional order of magnitude would allow for more thorough analysis of how translocation duration and signal intensity respond to variations in chemical and physical properties of the system. The results of that analysis would help determine whether events were virus translocations.

Our first experiments show that nanopores can detect John Cunningham Virus translocations, and they allow for future research to further refine the nanopore sensor so that it can more consistently detect virus translocations, and so that the shapes of its signals can offer insight into the physical properties of the spherical particle being translocated.

# Bibliography


[1] John L. Anderson. "Colloid Transport by Interfacial Forces". In: *Annual Review of Fluid Mechanics* 21 (Jan. 1989), pp. 61–99.

[2] Sven H. Behrens and David G. Grier. "The Charge of Glass and Silica Surfaces". In: *Journal of Chemical Physics* 115 (2001), pp. 6716–6721.

[3] Sergey M. Bezrukov, Alexander M. Berezhkovskii, and Atilla Szabo. "Diffusion Model of Solute Dynamics in a Membrane Channel: Mapping onto the Two-Site Model and Optimizing the Flux". In: *Journal of Chemical Physics* 127 (2007).

[4] Lyderic Bocquet and Elisabeth Charlaix. "Nanofluidics, from Bulk to Interfaces". In: *Chemical Society Reviews* 39.3 (2010), pp. 1073–1095.

[5] S. Chandrasekhar. "Stochastic Problems in Physics and Astronomy". In: *Reviews of Modern Physics* 15.1 (1943).

[6] R. W. DeBlois and C. P. Bean. "Counting and Sizing of Submicron Particles by the Resistive Pulse Technique". In: *American Institute of Physics: The Review of Scientific Instruments* 41.7 (July 1970), pp. 909–916.

[7] Cees Dekker. "Solid State Nanopores". In: *Nature Nanotechnology* 2 (Mar. 2007), pp. 209–215.

[8] Peter Hanggi, Peter Talkner, and Michal Borkovec. "Reaction Rate Theory: Fifty Years after Kramers". In: *American Physical Society: Reviews of Modern Physics* 62.2 (Apr. 1990), pp. 251–342.

[9] Laetitia Jubin et al. "Dramatic Pressure-Sensitive Ion Conduction in Conical Nanopores". In: *Proceedings of the National Academy of Sciences* 115.16 (2018), pp. 4063–4068.

[10] Joel Koplik, Jayanth R. Banavar, and Jorge F. Willemsen. "Molecular dynamics of Poiseuille flow and moving contact lines". In: *Physical Review Letters* 60.13 (1988), pp. 1282–1285.

[11] M. S. Maginnis and W. J. Atwood. "JCV: An Oncogenic in Animals and Humans?" In: *Seminars in Cancer Biology* 19.4 (2009), pp. 261–269.

[12] Angus McMullen et al. "Stiff Filamentous Virus Translocations through Solid-State Nanopores". In: *Nature Communications* 5.4171 (June 2014).

[13] Mirna Mihovilovic, Nicholas Hagerty, and Derek Stein. "Statistics of DNA Capture by a Solid-State Nanopore". In: *Physical Review Letters* 110.2 (2013).

[14] nanoComposix. "100 nm Silica Non-Functionalized Nanospheres, NanoXact Silica Certificate of Analysis. Lot Number: JEA0234". URL: https://tools.nanocomposix.com:48/cdn/coa/Silica/Silica-100nm-JEA0234.pdf?1061616.

[15] nanoComposix. "20 nm Silica Nanospheres, NanoXact Certificate of Analysis. Lot Number: JRC0080". URL: https://tools.nanocomposix.com:48/cdn/coa/Silica/Silica-20nm-5mg_mL-JCR0080.pdf?106%20645.

[16] nanoComposix. "50 nm Silica Nanospheres, Silica, NanoXact Certificate of Analysis. Lot Number: JEA0293". URL: https://tools.nanocomposix.com:48/cdn/coa/Silica/Silica-50nm-JEA0293.pdf?106%20001.

[17] Calin Plesa et al. "Fast Translocation of Proteins through Solid State Nanopores". In: *Nano Letters* 13 (2013), pp. 658–663.

[18] E. M. Purcell. "Life at Low Reynolds Number". In: *American Journal of Physics* 45.3 (1977).

[19] Juan M. Romero, O. Gonzalez-Gaxiola, and Chacon-Acosta. "Exact Solutions to Fick-Jacobs Equation". In: *International Journal of Pure and Applied Mathematics* 82.1 (2013), pp. 41–52.

[20] G. E. Uhlenbeck and L. S. Ornstein. "On the Theory of Brownian Motion". In: *Physical Review* 36 (Sept. 1930), pp. 823–841.

[21] Ming Chen Wang and G. E. Uhlenbeck. "On the Theory of Brownian Motion II". In: *American Physical Society: Reviews of Modern Physics* 17.2–3 (July 1945), pp. 323–342.